scientific reports

OPEN

Bottom-up plasma-enhanced atomic layer deposition of SiO_2 by utilizing growth inhibition using NH_3 plasma pre-treatment for seamless gap-fill process

Yoenju Choi[1,2], Taehoon Kim[2], Hangyul Lee[2], Jusung Park[2], Juhwan Park[2], Dongho Ryu[2] & Woojin Jeon[1]✉

The design-rule shrinkage in semiconductor devices is a challenge at every step of the integration process. In the gap-fill process for isolation, the seam and void formation cannot be suppressed by using a deposition process, which even has excellent step coverage. To achieve seamless gap fill in the high-aspect-ratio structure, which has a non-ideal etch profile such as a negative slope, the deposition process should be able to realize the "bottom-up growth" behavior. In this work, the bottom-up growth of a SiO_2 plasma-enhanced atomic layer deposition (PE-ALD) process in a trench structure was investigated by using a growth inhibition process employing plasma treatment. N_2 and NH_3 plasma pre-treatments were employed to suppress the growth of the SiO_2 PE-ALD process without any contamination, and the inhibition mechanism was investigated by performing surface chemistry analyses using X-ray photoelectron spectroscopy. Furthermore, the gap-fill characteristics of the SiO_2 PE-ALD process were examined, depending on the process conditions of NH_3 plasma pre-treatment, by performing cross-sectional field emission scanning electron microscopy measurements. Finally, a seamless gap-fill process in a high-aspect-ratio trench pattern was achieved by the bottom-up growth behavior of SiO_2 PE-ALD using NH_3 plasma pre-treatment.

Design rule shrinkage is a crucial requirement for increasing the integration density in semiconductors. To achieve a device with a reduced design rule, not only the patterning processes, such as lithography and etching, but also the isolation between actives, where the channel is located, is important to ensure robust device operation[1–6]. In this regard, isolation processes, such as shallow trench isolation, contact holes, channel hole oxides, and inter-metal dielectrics, have become important for obtaining cutting-edge semiconductor devices[2,7–10]. However, the difficulty of the isolation process increases with an increased aspect ratio of the structure and decreased space between actives (less than tens of nanometers) having a fixed depth (~ 1 μm). Therefore, a deposition process with excellent step coverage capability that can fill the space between actives without seam or void formation should be developed: this is one of the characteristics of the deposition process and is called "gap-fill characteristics." In this regard, atomic layer deposition (ALD) has been employed as a gap-fill process using SiO_2 thin films[2,7–15]. The ALD process exhibits self-limiting growth behavior induced by the chemisorption of a precursor at the surface of the substrate, resulting in a step coverage of over 95%. However, the excellent step coverage of the ALD process induces the formation of seams or voids[9,14]. In the case of a high-aspect-ratio pattern with an ideal etch profile and a positive slope, the ALD process can fill the structure. However, the real etch profile of a high-aspect-ratio pattern would have a negative slope, resulting in tapering or bowing shapes owing to process difficulty[7,16]. Where the sidewall of the trench or hole has a negative slope, the conformal SiO_2 film deposition induces the formation of seams or voids. In other words, the excellent step coverage characteristics of the deposition process hinder the gap-fill characteristics.

[1]Department of Advanced Materials Engineering for Information and Electronics, and Integrated Education Program for Frontier Science and Technology (BK21 Four), Kyung Hee University, Yongin, Gyeonggi 17104, Korea. [2]Semiconductor R&D Center, WONIK IPS Co., Ltd., Pyeongtaek, Gyeonggi 17709, Korea. ✉email: woojin.jeon@khu.ac.kr

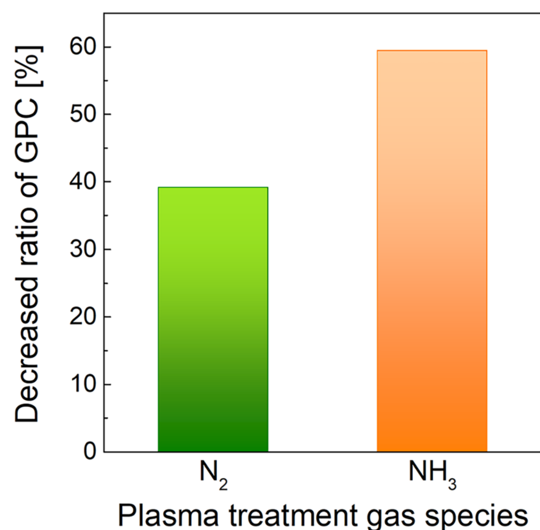

Figure 1. Decreased GPC ratio of SiO_2 PE-ALD with N_2^* and NH_3^* compared with the no inhibitor case.

Gas species	GPC (nm/cycle)	Decreased ratio (%)
No inhibitor	0.064	
N_2	0.039	39.1
NH_3	0.026	59.4

Table 1. GPC of SiO_2 PE-ALD with various inhibition conditions and decreased ratio compared with the no inhibitor case.

Therefore, in the high-aspect-ratio pattern, higher growth rate at the bottom region of the trench than at the top region and surface would be favorable for filling the pattern without the formation of seams or voids. This is called "bottom-up growth"[2,17,18]. However, most of the deposition processes have a relatively higher growth rate in the top region of the trench ("top region") because the concentration of the reactant is higher in this region[19]. Hence, the introduction of an inhibitor, which can suppress the growth of thin film deposition, was investigated to control the growth rate in this region. Among the various inhibition techniques, the plasma process is adequate for demonstrating the inhibition effect only in the top region[20,21], because the plasma generally has a large concentration gradient in the high-aspect-ratio pattern[19,22]. However, plasma treatment can induce N or C contamination depending on the gas species, which can contribute to defects in the thin film.

Based on these considerations, the bottom-up growth of SiO_2 thin film deposition by employing a surface modification process via plasma treatment for the gap-fill process was investigated in this work. Plasma treatment was conducted by employing gases having a simple structure, namely, N_2 and NH_3, to avoid contamination. The inhibitory effect of the plasma treatment on the growth of the SiO_2 thin film was examined. Moreover, the mechanism involved in this inhibitory effect was evaluated. Eventually, the bottom-up growth behavior and gap-fill characteristics were investigated by employing plasma pre-treatment.

Results and discussion

Figure 1 and Table 1 present the growth inhibition effect of plasma pre-treatment depending on the gas species, namely, N_2 and NH_3. Before the plasma-enhanced ALD (PE-ALD) SiO_2 sequence was implemented, 1 s of plasma pre-treatment was performed for each gas species. The growth rate (growth per cycle, GPC) of PE-ALD SiO_2 was 0.064 nm/cycle without any plasma pre-treatment, and it decreased to 0.039 and 0.026 for N_2 plasma pre-treatment (N_2^*) and NH_3 plasma pre-treatment (NH_3^*), respectively. The decreased GPC ratios compared with the case of no inhibitor were 39.1, and 59.4% for N_2^* and NH_3^*, respectively. The difference in the inhibition effect was attributed to the difference in the reactivity between N_2^* and NH_3^*. As NH_3 consists of relatively weak chemical bonding, N–H, a relatively large number of radicals might be induced, resulting in higher growth inhibition in the PE-ALD SiO_2.

The chemical status and impurity incorporation during plasma pre-treatment were investigated using X-ray photoelectron spectroscopy (XPS). Figure 2a shows the depth profiles of deposited SiO_2 thin films with no treatment, N_2^*, and NH_3^*. In all cases, the deposited SiO_2 thin films had identical depth profiles for all elements, regardless of pre-treatment. To confirm the impurity incorporation by employing plasma pre-treatment, the depth profiles of C and N are depicted in Fig. 2b, which is a magnification of those in Fig. 2a. As shown in Fig. 2b, the concentrations of both C and N are less than 2 at.%, which is the detection limit of the XPS measurement.

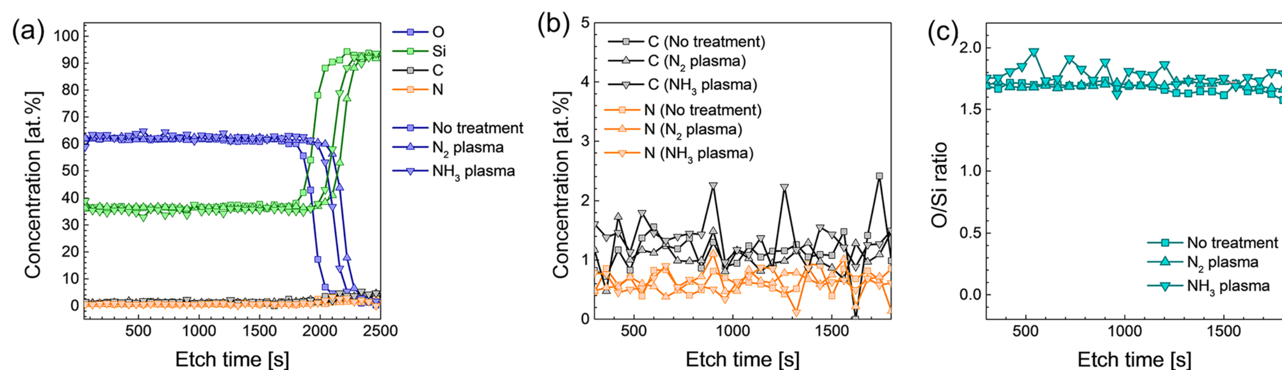

Figure 2. (**a**) Depth profiles of O, Si, C, and N; (**b**) depth profiles of C and N; (**c**) oxygen stoichiometry (O/Si ratio) of the thin films.

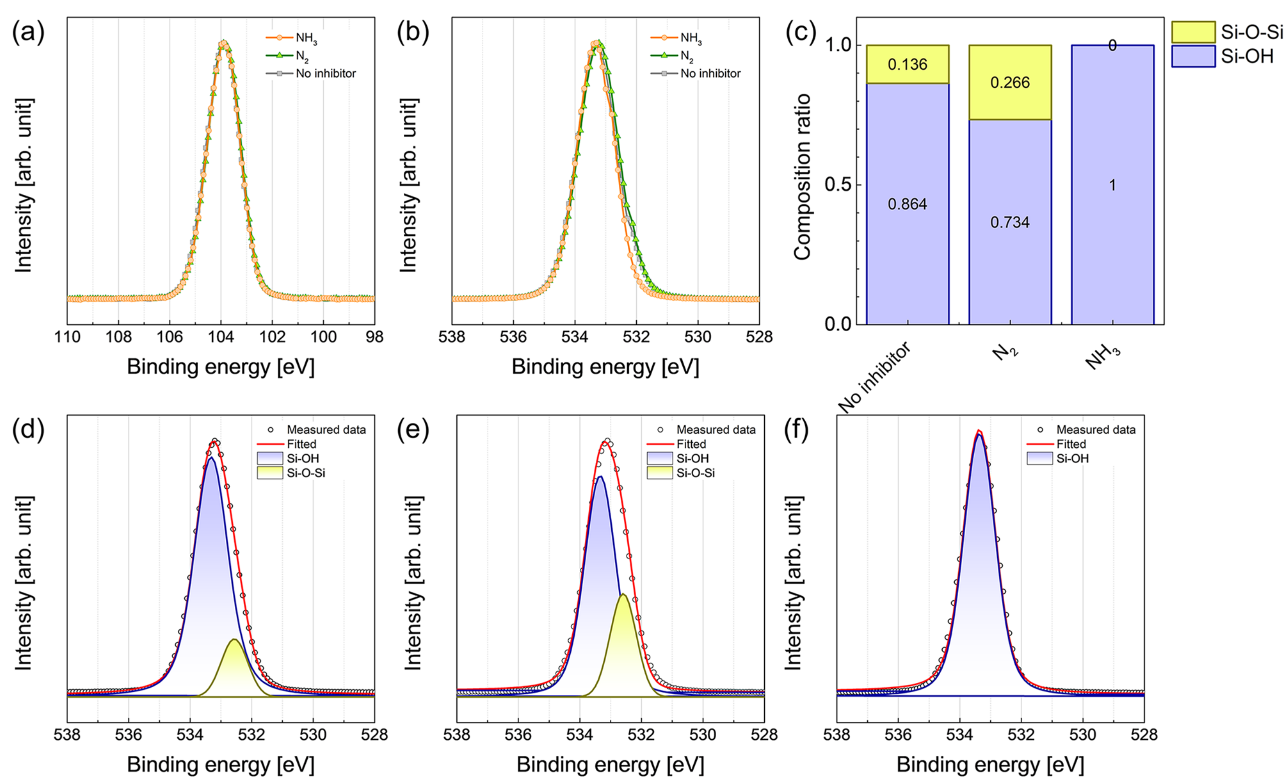

Figure 3. XPS profiles of (**a**) Si2*p*, and (**b**) O1*s* of SiO_2 thin films. (**c**) Composition ratio of Si–O–Si and Si–OH bonding in O1*s* XPS spectra. Deconvoluted XPS O1*s* peaks of SiO_2 thin films with (**d**) no inhibitor, (**e**) N_2^*, and (**f**) NH_3^*.

In addition, no increment in C or N concentration is observed by employing plasma pre-treatment. Because of the almost identical depth profiles and negligible C and N concentrations, plasma pre-treatment can inhibit the growth of SiO_2 PE-ALD without inducing any contamination or residue. Moreover, the stoichiometry of the deposited SiO_2 thin films was calculated (Fig. 2c). In the case of SiO_2 without pre-treatment, the O/Si ratio was 1.68 with homogeneity in the depth direction (standard deviation of 0.033). A relatively low O/Si ratio was attributed to the different sputtering yields between Si and O (lighter atom tends to easily sputtered out) during the etching for the depth profiling. The SiO_2 thin film with N_2^* had an O/Si ratio of 1.70 with a high uniformity (standard deviation of 0.017). In contrast, the O/Si ratio in the SiO_2 thin film with NH_3^* was relatively high at 1.78, with a slightly large fluctuation in the depth direction and a standard deviation of 0.075.

The chemical states of the deposited films were also investigated. Figure 3a shows the Si2*p* XPS spectra of the SiO_2 thin films. All the spectra have identical profiles and only consist of Si–O bonding, corresponding to a binding energy of 103.8 eV[23]. However, in the O1*s* XPS spectra, as shown in Fig. 3b, a difference is observed depending on the plasma pre-treatment. In the case of no inhibitor and N_2^*, a shoulder at approximately 532 eV is observed, which is evidence that the peak at the lower binding energy contributed to the spectra. From the O1*s* spectra, the composition of two bondings on the surface was evaluated (Fig. 3c) by the deconvolution to peaks at 532.6

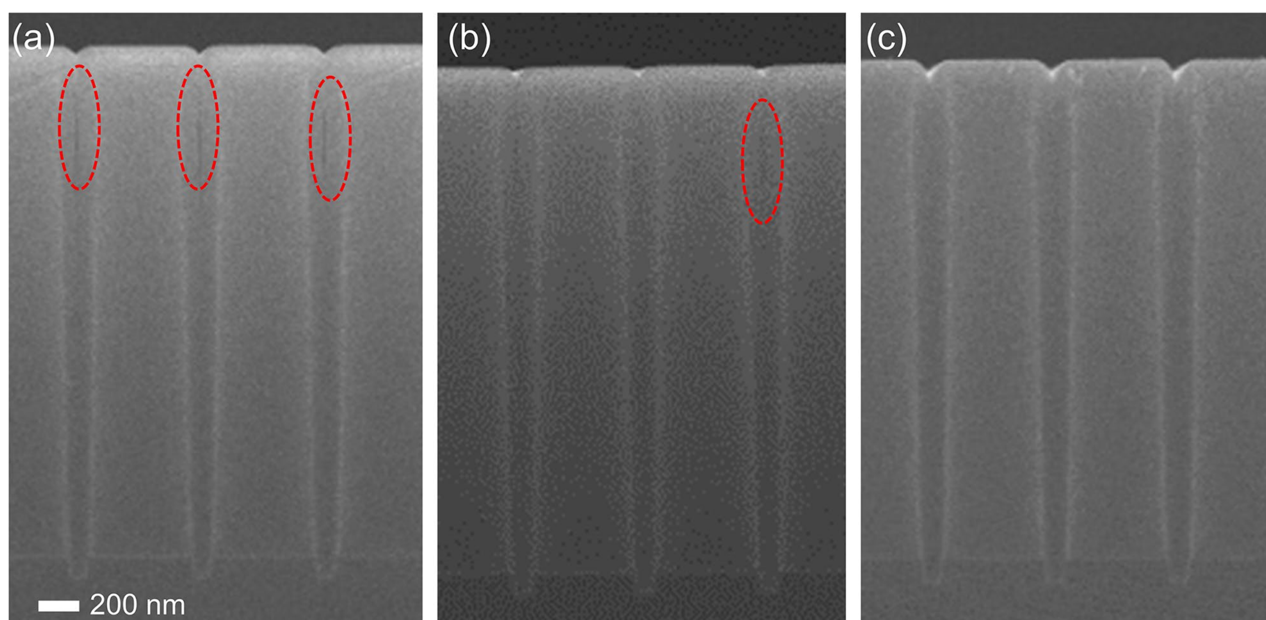

Figure 4. Cross-sectional field-emission scanning electron microscopy (FE-SEM) images of the trench pattern (aspect ratio of 25:1 with an opening size and a depth of 200 nm and 2.5 µm, respectively) after conducting SiO_2 PE-ALD with (**a**) no inhibitor, (**b**) N_2^*, and (**c**) NH_3^*.

and 533.5 eV corresponding to the Si–O–Si and Si–OH bonding, respectively (Fig. 3d–f)[23]. These two bonds are strongly related to the SiO_2 PE-ALD process. The Si–O–Si bond corresponds to the covalent bond of SiO_2. The Si–OH bonding is the surface termination of the SiO_2 thin film. In the ALD process, the precursor chemisorbs on the surface through a ligand exchange reaction with the functional group on the surface, which is called "anchoring site," and only the chemisorbed precursor participates in the film formation reaction with the reactant, resulting in the self-limiting growth characteristics. The surface functional groups and their chemistry and density strongly influence the growth behavior in the ALD process. In the SiO_2 PE-ALD process, the Si–OH bonding, generally called the hydroxyl group, contributes to the ligand exchange reaction with diisopropylamino silane (DIPAS) (Si precursor)[15,24]. The Si–OH bonding on the surface is changed to $Si_{(from\ the\ surface)}–O–Si_{(from\ the\ DIPAS)}–H_3$ during the precursor feeding step[24]. After the reactant feeding step and the reactant purge step, the Si–OH bonding on the surface is recovered and participates in the chemisorption of DIPAS. Therefore, after the SiO_2 PE-ALD process is conducted, the surface consists of Si–OH bonds. In the case of SiO_2 deposition with NH_3^*, the surface consists of only Si–OH bonding, implying that all the chemisorbed precursors fully react with the reactant and change into Si–OH bonding. Moreover, the passivated Si–OH bonding during the NH_3^* step recovers to Si–OH bonding during the SiO_2 PE-ALD process, resulting in growth inhibition without N contamination. In contrast to the case of NH_3^*, the no inhibitor and N_2^* cases exhibit Si–O–Si bonding ratios of 0.136 and 0.266, respectively. The Si–O–Si bonding on the surface might originate from the remaining $Si_{(from\ the\ surface)}–O–Si_{(from\ the\ DIPAS)}–H_3$ or the covalent bonding of SiO_2. Both cases indicate that the recovery of the Si–OH bonding during the reactant feeding and purge steps was suppressed or insufficient.

The gap-fill characteristics depending on the plasma pre-treatment were confirmed (Fig. 4). In the case of no inhibitor, voids in the trench are clearly observed, as shown in Fig. 4a. Although N_2^* inhibits the growth of SiO_2, the void formed by the imperfection gap fill remains (Fig. 4b). Only in the case of NH_3^*, a perfect gap-fill characteristic is obtained (Fig. 4c). Consequently, the inhibition of the growth of SiO_2 can enhance the gap-fill characteristics.

Further investigation of the growth inhibition effect by NH_3^* was performed. First, growth inhibition depending on the ratio of NH_3^* was evaluated. A treatment ratio of 0.1 indicates that the super-cycle consists of one cycle of NH_3^* and nine cycles of SiO_2 PE-ALD (refer to Fig. 5). In the same manner, a treatment ratio of 0.5 means a super-cycle consists of one cycle of NH_3^* and one cycle of SiO_2 PE-ALD. As shown in Fig. 6, the growth rate gradually decreases, displaying an almost linear relationship with an increasing treatment ratio, indicating that growth inhibition by employing NH_3^* originated from the chemical inactivation of the Si–OH functional groups. The decreased Si–OH functional group density on the surface induces a decrease in the amount of chemisorbed Si precursor, resulting in a decrease in the growth rate. Moreover, the change in the growth rate depending on the NH_3 flow rate during NH_3^* was examined (Fig. 7a). The NH_3 flow rate is related to the concentration of radicals formed in NH_3^*. When the NH_3 flow rate was 50 standard cubic centimeter (sccm), the inhibition effect of NH_3^* was slightly reduced from 0.026 nm/cycle to a growth rate of 0.031 nm/cycle. The decreased inhibition effect at an NH_3 flow rate of 50 sccm induced a deteriorated gap-fill characteristic, as shown by the void formation in Fig. 7b. As the NH_3 flow rate increasing to 100 sccm, the GPC was decreased to 0.026 nm/cycle, which is saturated value, and the seam-free gap-fill growth was observed (Fig. 7c,d). Furthermore, the time for NH_3^* was varied at 500 sccm and the treatment ratio was 0.5. As shown in Fig. 7e, the growth rate increases from 0.026 nm/cycle to 0.36 and 0.45 nm/cycle as the treatment time decreases from 1.0 s to 0.5 and 0.25 s, respectively.

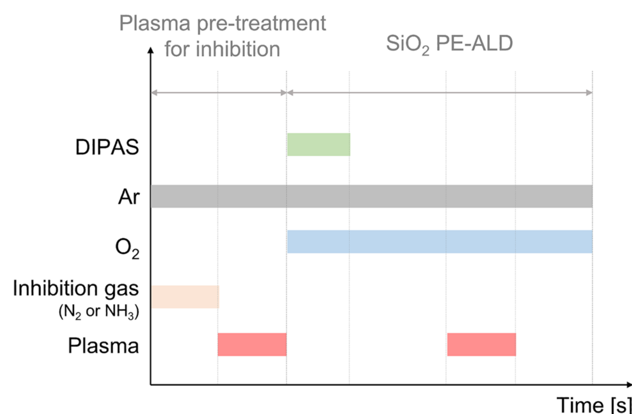

Figure 5. Schematic diagram of the process sequence constitution.

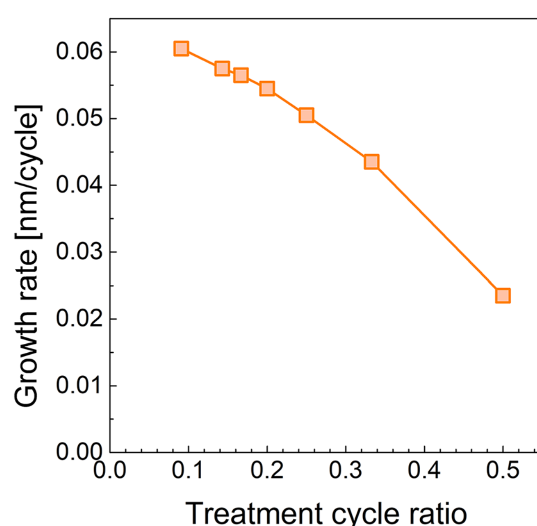

Figure 6. GPC change with respect to the treatment cycle ratio of the plasma pre-treatment to the total PE-ALD sequence as shown in Fig. 5.

The growth rate of 0.45 nm/cycle at a treatment time of 0.25 s is comparable to that of 0.039 nm/cycle for N_2^*. This relatively high growth rate results in defective gap-fill characteristics (Fig. 7f). In the case of the treatment time of 0.5 and 1.0 s, the seam was not observed (Fig. 7g,h). In this regard, the difference in the stoichiometry (Fig. 2c) and surface termination can be ascribed to the change in the amount of the chemisorbed precursor. Even though the reactant was overdosed during the ALD process, the stoichiometry of the deposited thin film was strongly influenced by the density of the chemisorbed precursor on the substrate[25]. The higher O/Si ratio in the SiO_2 thin film prepared using NH_3^* implies that the density of chemisorbed DIPAS decreased. Moreover, the recovery of surface termination to Si–OH (Fig. 3f) was facilitated by a relatively higher oxygen source ratio than the chemisorbed precursor.

These results confirmed that NH_3^* can suppress the growth of SiO_2 thin films deposited via PE-ALD by inactivating the Si–OH functional groups on the surface. NH_3^* induces bottom-up growth behavior during the SiO_2 PE-ALD process. In the case of no inhibitor (Fig. 8a–d), the introduced Si precursors were chemisorbed on the top and bottom of the trench-patterned structure (Fig. 8a) and exhibited the same growth rate. However, after NH_3^* was performed (Fig. 8e–j), the inhibition only affected the top of the pattern (Fig. 8e), where the NH_3^* was exposed; in turn, the growth was only inhibited on the surface and the top region (Fig. 8g). Therefore, the growth rate difference between the top and bottom regions of the pattern demonstrated bottom-up growth behavior (Fig. 8j). The inhibition of SiO_2 on the top region of the pattern by the NH_3^* treatment was confirmed by performing a cross-sectional SEM analysis of the trench pattern (Fig. 9). For NH_3^*, the thickness of the deposited SiO_2 thin film on surface was 18.8 nm, whereas the thickness of SiO_2 deposited on the side was 32.5 nm. As the deposition was conducted, the bottom-up growth of SiO_2 in the trench pattern was observed. Furthermore, the bottom-up gap-fill characteristic was examined in a trench pattern with a small opening size and high aspect-ratio (opening and depth of 200 nm and 2.5 µm, respectively) after conducting SiO_2 gap-fill using NH_3^* by using the transmission electron microscopy (TEM) observation (Fig. 10). As shown in Fig. 10a, the trench was filled with SiO_2 from the bottom of the pattern to the top region of the pattern. The thicknesses

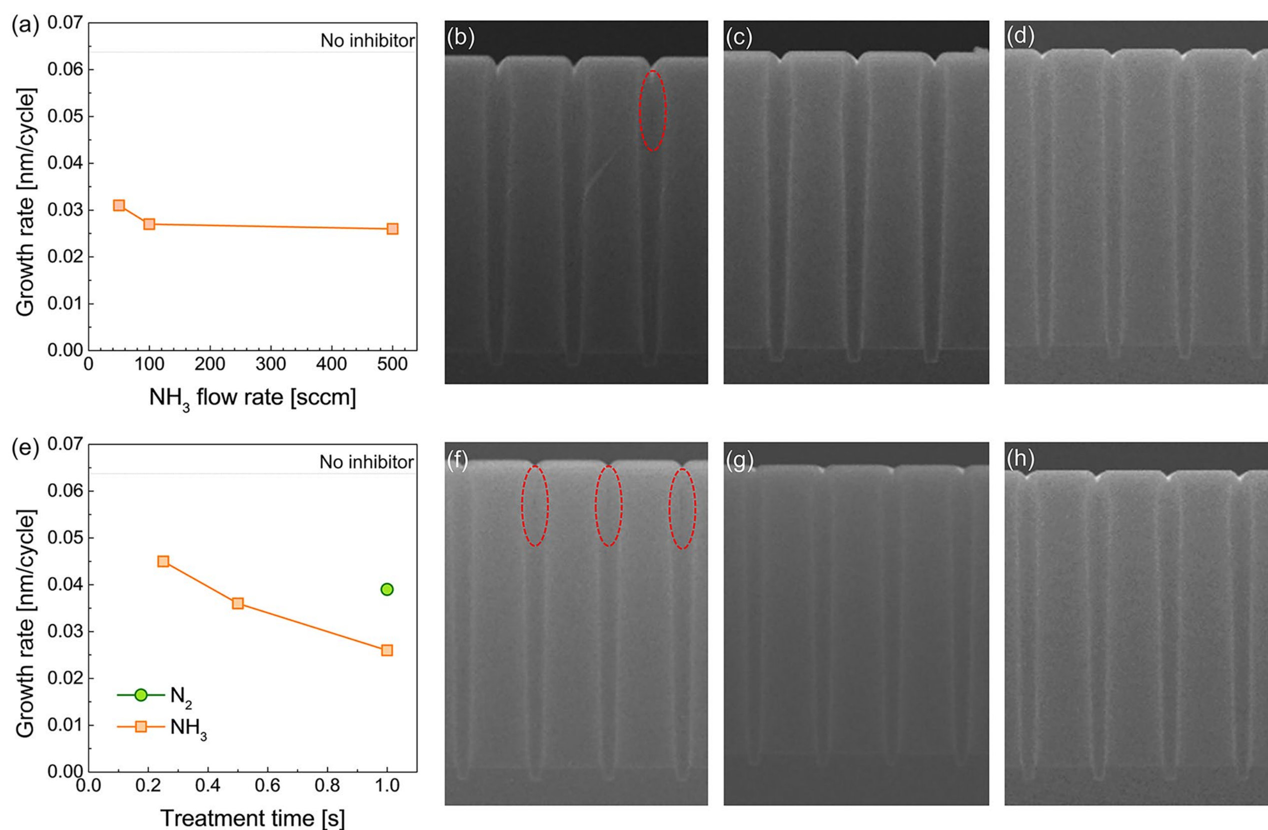

Figure 7. (**a**) GPC of SiO_2 PE-ALD using NH_3^* with various NH_3 flow rates. Cross-sectional FE-SEM images of the trench pattern after deposition of SiO_2 thin film using NH_3^* with NH_3 flow rate of (**b**) 50, (**c**) 100, and (**d**) 500 sccm. (**e**) GPC of SiO_2 PE-ALD using NH_3^* with various treatment times. N_2^* with treatment time of 1 s is represented by the green dot for comparison. Cross-sectional FE-SEM images of the trench pattern after deposition of SiO_2 thin film using NH_3^* with treatment time of (**f**) 0.25, (**g**) 0.5, and (**h**) 1.0 s.

of SiO_2 on the side where the region not filled (Fig. 10b) was gradually decreased from the bottom of 89.5 nm to the top of 56.6 nm also indicating the bottom-up characteristic. Moreover, at the negative sloped area near the top area of the trench (Fig. 10c), the deposited SiO_2 film thickness gradually increased from the top (35.6 nm) to the bottom (58.5 nm). This is because of the relatively poor step coverage of NH_3^* treatment. Due to the negative slope, the NH_3^* was hard to reach on the surface of the side near the top area of the trench, inducing a gradient of the Si–OH functional groups on the surface. From the images of Fig. 10d,e, no seam was observed even in the TEM observation, indicating that the bottom-up gap-fill characteristics were achieved.

To confirm the seamless gap-fill characteristics more accurately, wet etching (using an etchant of diluted HF at a ratio of 200:1 for 60 s) was conducted, followed by cross-sectional SEM analyses. As shown in Fig. 11a, the seam propagates to the bottom of the pattern because of the infiltrated etchant in the case of the SiO_2 thin film deposited with no inhibitor. In contrast, in the case of NH_3^*, no seam is observed and only the surface is etched out with notch shapes (Fig. 11b). This profile indicates that no holes or voids are present where the etchant can infiltrate. In other words, perfect bottom-up growth was achieved by using NH_3^*. Owing to the bottom-up growth behavior, the gap-fill characteristics were significantly enhanced. The SiO_2 PE-ALD process with NH_3^* was performed on the patterned structure, which had a varied trench opening size (Fig. 11c). On the large-opening-size trench, the trench was not fully filled, but it showed the bottom-up growth behavior; the level of the end point of the unfilled region (indicated by red circles in Fig. 11c) gradually moved upward to the surface. This bottom-up growth resulted in perfect gap-fill characteristics in the narrowest trench. Moreover, bottom-up growth was observed even on the surface after completion of the gap fill of the trench (blue circles in Fig. 11c).

Conclusion

The bottom-up growth of the SiO_2 PE-ALD process was investigated by employing an inhibitor of NH_3 plasma pre-treatment to demonstrate seam- and void-less gap fill on an extremely high-aspect-ratio pattern. Plasma pre-treatment with N_2 or NH_3 gas effectively decreased the growth of SiO_2 PE-ALD without any contamination because of the suppression of the chemisorption of DIPAS on the substrate surface. The plasma concentration gradient in the trench structure induced a growth rate difference between beneath the trench and the surface, resulting in the relationship between enhanced gap-fill characteristics and the plasma pre-treatment process condition, which has a higher growth inhibitory effect. Owing to the inhibition effect of NH_3^*, the bottom-up growth behavior of SiO_2 PE-ALD was successfully implemented in the trench structure. Finally, a seamless gap-fill process was achieved in the high-aspect-ratio pattern.

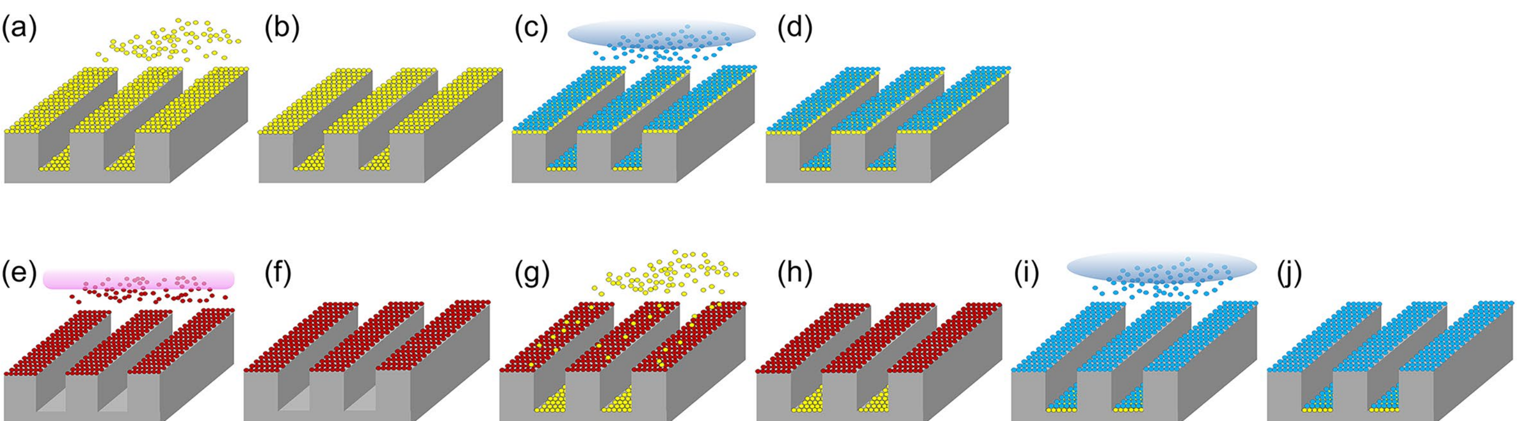

Figure 8. Schematic diagram of the SiO_2 PE-ALD sequence consisting of (**a**) precursor feeding, (**b**) Ar purge, (**c**) O_2 plasma, and (**d**) Ar purge. Schematic diagram of SiO_2 PE-ALD using NH_3^* sequence consisting of (**e**) NH_3 plasma, (**f**) Ar purge, (**g**) precursor feeding, (**h**) Ar purge, (**i**) O_2 plasma, and (**j**) Ar purge. To clearly describe the precursor chemisorption beneath the trench pattern and surface, the precursor chemisorbed on the sidewall of trench is omitted.

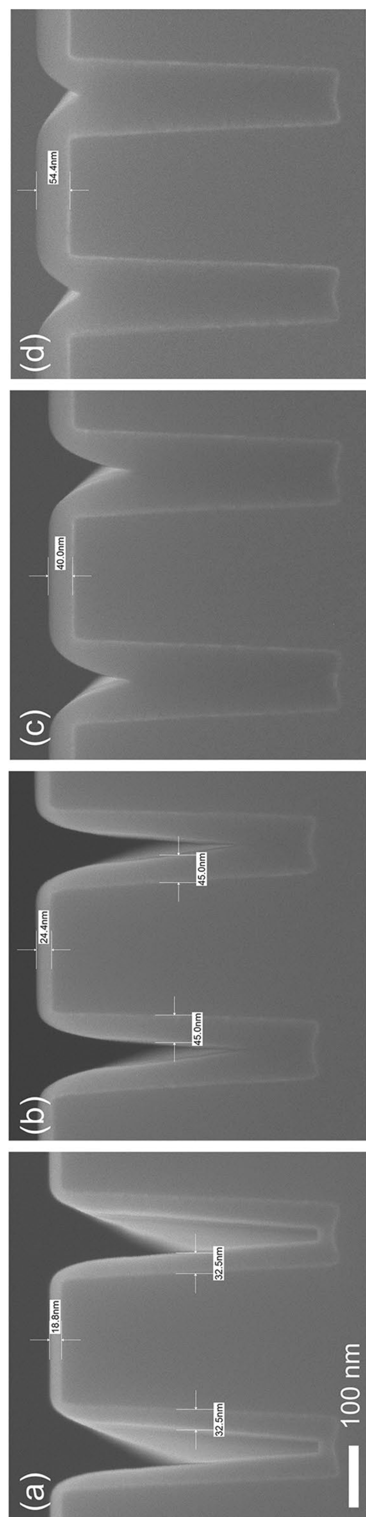

Figure 9. Cross-sectional FE-SEM images of the trench pattern (opening and depth of 150 and 400 nm, respectively) after conducting SiO_2 PE-ALD using NH_3^* for (**a**) 750, (**b**) 1000, (**c**) 1500, and (**d**) 2000 cycles.

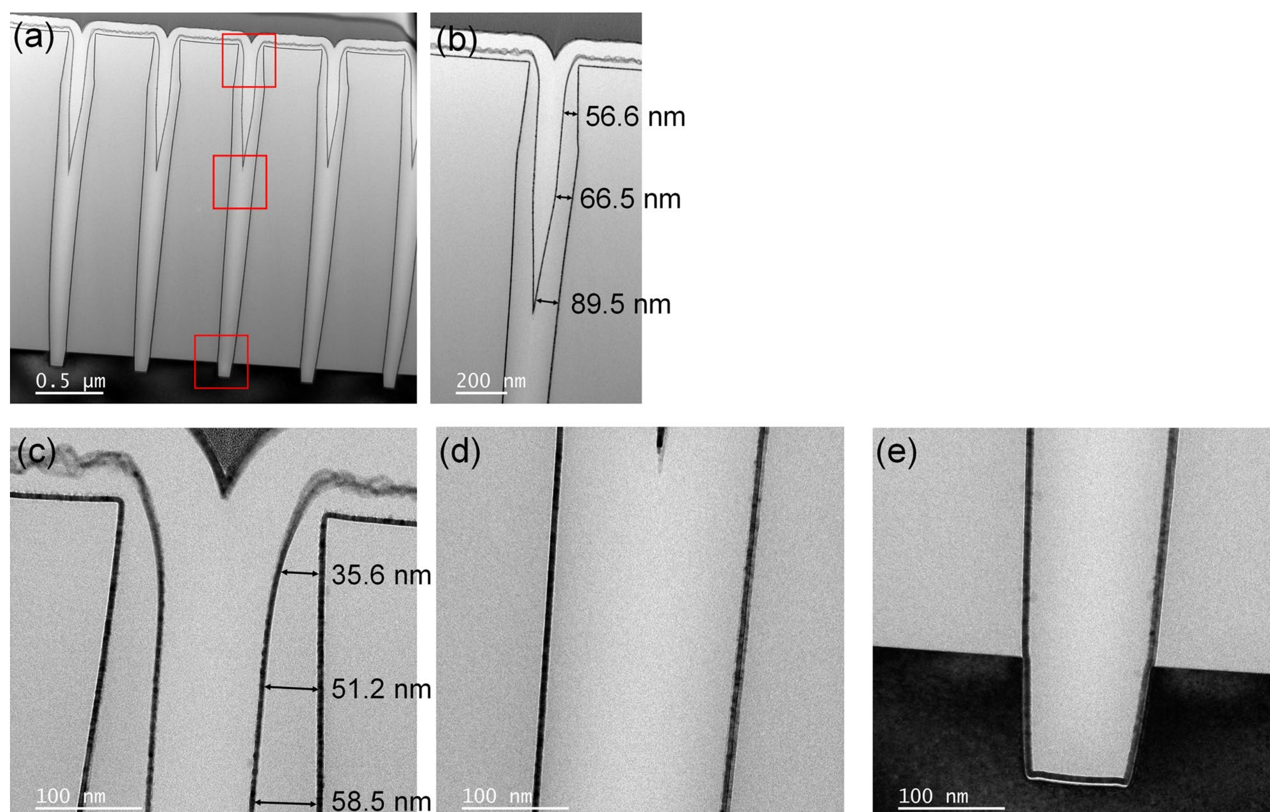

Figure 10. (**a**) Cross-sectional TEM image of the trench patterns (opening and depth of 200 nm and 2.5 μm, respectively) after conducting the SiO_2 PE-ALD using NH_3^*. (**b**) 20,000× magnified image of trench opening area, and (**c**–**e**) 80,000× magnified images of (**c**) trench opening area, (**d**) center of trench, and (**e**) bottom of trench (depicted as red boxes in (**a**)), respectively.

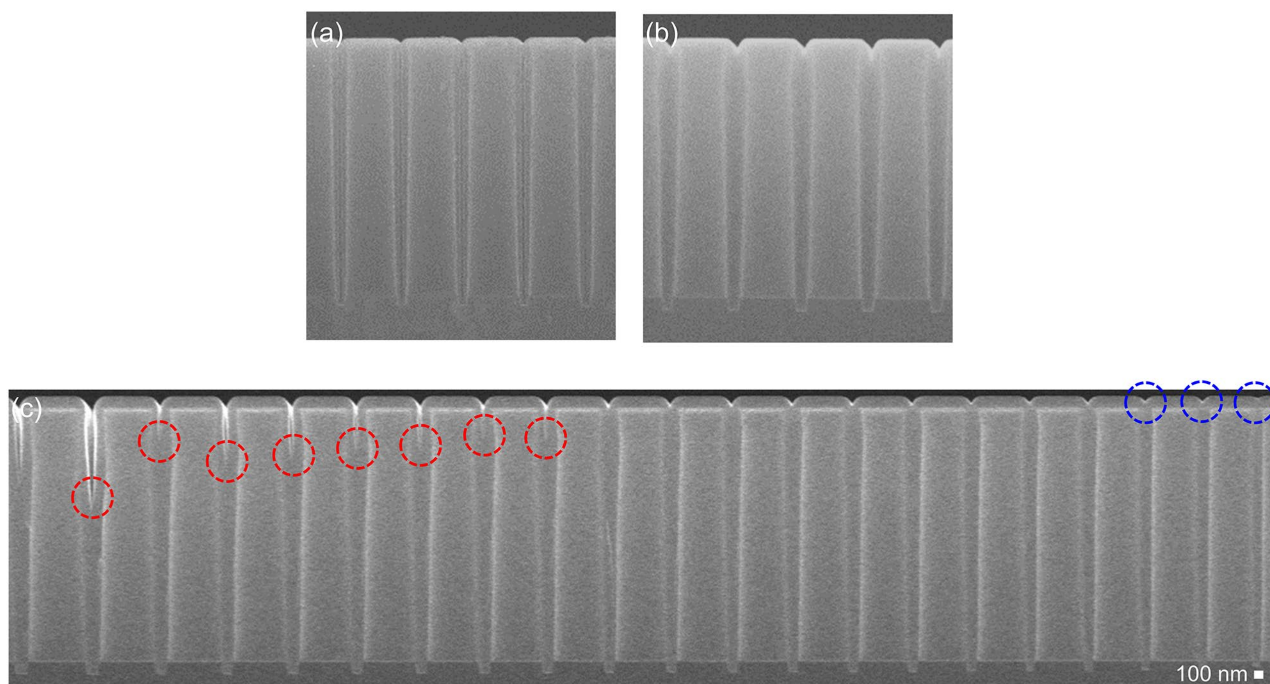

Figure 11. Cross-sectional FE-SEM images of the trench pattern (opening and depth of 200 nm and 2.5 μm, respectively) after conducting SiO_2 PE-ALD with (**a**) no inhibitor and (**b**) NH_3^*, followed by wet etching (diluted HF of 200:1 for 60 s). (**c**) Cross-sectional FE-SEM images after conducting SiO_2 PE-ALD with NH_3^* on the trench pattern with a depth of 3 μm and an opening size varying from 300 (left) to 100 (right) nm.

Methods

SiO_2 thin films were deposited by applying PE-ALD)(MAHA_AL, Wonik IPS) using DIPAS as the Si precursor and O_2 plasma with capacitively coupled plasma at a frequency of 13.56 MHz as the oxygen source. The Si precursor was introduced using a bypass-type source delivery system with a heated canister at 50 °C and an Ar flow as the carrier gas. The PE-ALD process temperature was 50 °C, and the sequence consisted of precursor feeding, Ar purging, O_2 plasma with a plasma power of 100 W, and Ar purging for 3, 5, 1, and 5 s.

Plasma pre-treatment was conducted prior to the SiO_2 PE-ALD sequence to inhibit the growth of SiO_2 PE-ALD. The plasma pre-treatment sequence consisted of gas feeding and plasma treatment, each for 1 s. Two types of gases, N_2 and NH_3, were employed, and the plasma pre-treatment was conducted at a process temperature of 50 °C with a plasma power of 100 W. The total deposition sequence is shown in Fig. 5.

The thicknesses of the deposited SiO_2 thin films were measured by applying ellipsometry (Aleris, KLA-Tencor). The depth profiles, compositions, and chemical states of the thin films were analyzed using XPS (NEXSA, ThermoFisher Scientific). The gap-fill characteristics of the SiO_2 PE-ALD process were examined by performing cross-sectional SEM (FE-SEM, JSM 760F, JEOL) and TEM (JEM-F200, JEOL) in trench structures having a depth of 1 µm and opening sizes varying from 100 to 300 nm.

Data availability

All data generated or analysed during this study are included in this published article.

Received: 30 May 2022; Accepted: 9 September 2022
Published online: 21 September 2022

References

1. Clark, R. *et al.* Perspective: New process technologies required for future devices and scaling. *APL Mater.* **6**, 058203 (2018).
2. Tavernier, A., Favennec, L., Chevolleau, T. & Jousseaume, V. Innovative gap-fill strategy for 28 nm shallow trench isolation. *ECS Meeting Abstracts* **MA2012-01**, 748 (2012).
3. Wu, Q., Li, Y., Zhu, X. & Yu, S. The discussion of the typical BEOL design rules from 3 nm to 2 nm logic process with EUV and high NA EUV lithography. *IWAPS 2021—2021 5th International Workshop on Advanced Patterning Solutions* 5–8. https://doi.org/10.1109/IWAPS54037.2021.9671251 (2021).
4. Oniki, Y., Altamirano-Sánchez, E. & Holsteyns, F. (Invited) Selective etches for gate-all-around (GAA) device integration: Opportunities and challenges. *ECS Meeting Abstracts* **MA2019-02**, 1092–1092 (2019).
5. Sakai, K., Takanashi, K. & Sakai, T. Recent progress on spin-on inorganic materials. *IEEE International Symposium on Semiconductor Manufacturing Conference Proceedings* **2020-Decem**, 25–27 (2020).
6. Kim, S. S. *et al.* Review of semiconductor flash memory devices for material and process issues. *Adv. Mater.* https://doi.org/10.1002/adma.202200659 (2022).
7. Chen, Y. *et al.* Advanced HDP STI gap-fill development in 65 nm logic device. *ECS Trans.* **27**, 679–683 (2010).
8. Hatton, B. D. *et al.* Materials chemistry for low-k materials. *Mater. Today* **9**, 22–31 (2006).
9. Vassiliev, V. Y. ULSI gap filling with a thin CVD SiO_2-based insulator: A review. *Russ. Microlectron.* **31**, 224–231 (2002).
10. Schwartz, G. C. & Johns, P. Gap-fill with PECVD SiO_2 using deposition/sputter etch cycles. *J. Electrochem. Soc.* **139**, 927–932 (1992).
11. Vasilyev, VYu. Review—Atomic layer deposition of silicon dioxide thin films. *ECS J. Solid State Sci. Technol.* **10**, 053004 (2021).
12. Sakai, K., Takanashi, K. & Sakai, T. Recent progress on spin-on inorganic materials. *IEEE International Symposium on Semiconductor Manufacturing Conference Proceedings* **2020-Decem**, 2–4 (2020).
13. Sun, Y. & Wei, S. M. STI gap-fill technology and flowable CVD process application. *China Semiconductor Technology International Conference 2021, CSTIC 2021* 54–56. https://doi.org/10.1109/CSTIC52283.2021.9461477 (2021).
14. Nishimura, H., Takagi, S., Fujino, M. & Nishi, N. Gap-fill process of shallow trench isolation for 0.13 µm technologies. *Jpn. J. Appl. Phys. Part 1 Regul. Pap. Short Notes Rev. Pap.* **41**, 2886–2893 (2002).
15. Nam, T. *et al.* Low-temperature, high-growth-rate ALD of SiO_2 using aminodisilane precursor. *Appl. Surf. Sci.* **485**, 381–390 (2019).
16. Wormington, M. *et al.* X-ray critical dimension metrology solution for high aspect ratio semiconductor structures. In *Metrology, Inspection, and Process Control for Semiconductor Manufacturing XXXV* (eds Adan, O. & Robinson, J. C.) 27 (SPIE, 2021). https://doi.org/10.1117/12.2583966.
17. Wu, K., Lee, S., Banthia, V. & Hung, R. Improving Tungsten gap-fill for advanced contact metallization. *2016 IEEE International Interconnect Technology Conference/Advanced Metallization Conference, IITC/AMC 2016* 171–173. https://doi.org/10.1109/IITC-AMC.2016.7507721 (2016).
18. Akolkar, R. & Landau, U. Mechanistic analysis of the "bottom-up" fill in copper interconnect metallization. *J. Electrochem. Soc.* **156**, D351 (2009).
19. Arts, K., Deijkers, S., Puurunen, R. L., Kessels, W. M. M. & Knoops, H. C. M. Oxygen recombination probability data for plasma-assisted atomic layer deposition of SiO_2 and TiO_2. *J. Phys. Chem. C* **125**, 8244–8252 (2021).
20. Majhi, M. *Growth and Characterizations of SiO2 Thin Film on Silicon Substrates* (National Institute of Technology, 2013).
21. Lee, D. R., Lucovsky, G., Denker, M. S. & Magee, C. Nitrogen-atom incorporation at Si–SiO_2 interfaces by a low-temperature (300 °C), pre-deposition, remote-plasma oxidation using N_2O. *J. Vac. Sci. Technol. A Vac. Surf. Films* **13**, 1671–1675 (1995).
22. Knoops, H. C. M., Faraz, T., Arts, K. & Kessels, W. M. M. Status and prospects of plasma-assisted atomic layer deposition. *J. Vac. Sci. Technol. A* **37**, 030902 (2019).
23. Hashemi, A. & Bahari, A. Structural and dielectric characteristic of povidone–silica nanocomposite films on the Si (n) substrate. *Appl. Phys. A* **123**, 535 (2017).
24. Yang, J. H., Baek, S. B. & Kim, Y. C. Initial surface reaction of di-isopropylaminosilane on a fully hydroxyl-terminated Si (001) surface. *J. Nanosci. Nanotechnol.* **14**, 7954–7960 (2014).
25. Jeon, W., Cho, Y., Jo, S., Ahn, J.-H. & Jeong, S.-J. Wafer-scale synthesis of reliable high-mobility molybdenum disulfide thin films via inhibitor-utilizing atomic layer deposition. *Adv. Mater.* **29**, 1703031 (2017).

Acknowledgements

W. Jeon acknowledges support by Korea Evaluation Institute of Industrial Technology through Technology Innovation Program (No. 20017228).

Author contributions

The manuscript was written through contributions of all authors. All authors have given approval to the final version of the manuscript. Y.C., T.K., H.L., Jusung Park, and Juhwan Park performed thin film deposition, device fabrication, and characterization. D.R., and W.J. designed the experiment and co-wrote the paper. All of the authors discussed the results and commented on the paper.

Competing interests

The authors declare no competing interests.

Additional information

Correspondence and requests for materials should be addressed to W.J.

Reprints and permissions information is available at www.nature.com/reprints.

Publisher's note Springer Nature remains neutral with regard to jurisdictional claims in published maps and institutional affiliations.

Open Access This article is licensed under a Creative Commons Attribution 4.0 International License, which permits use, sharing, adaptation, distribution and reproduction in any medium or format, as long as you give appropriate credit to the original author(s) and the source, provide a link to the Creative Commons licence, and indicate if changes were made. The images or other third party material in this article are included in the article's Creative Commons licence, unless indicated otherwise in a credit line to the material. If material is not included in the article's Creative Commons licence and your intended use is not permitted by statutory regulation or exceeds the permitted use, you will need to obtain permission directly from the copyright holder. To view a copy of this licence, visit http://creativecommons.org/licenses/by/4.0/.

© The Author(s) 2022